LUND UNIVERSITY

Wideband Sparse Reconstruction for Scanning Radar

Y. ZHANG, A. JAKOBSSON, Y. ZHANG, Y. HUANG, AND J. YANG

Published in: IEEE Trans. Geoscience and Remote Sensing
doi:10.1109/TGRS.2018.2830100

Lund 2018

Mathematical Statistics
Centre for Mathematical Sciences
Lund University

Wideband Sparse Reconstruction for Scanning Radar

Yongchao Zhang, *Student Member, IEEE*, Andreas Jakobsson, *Senior Member, IEEE*, Yin Zhang, *Member, IEEE*, Yulin Huang, *Member, IEEE* and Jianyu Yang, *Member, IEEE*

***Abstract*— Recently, the generalized sparse iterative covariance-based estimation (SPICE) algorithm was extended to allow for varying norm constraints in scanning radar applications. In this work, we further this development, introducing a wideband dictionary framework, which can provide a computationally efficient estimation of sparse signals. The technique is formed by initially introducing a coarse grid dictionary constructed from integrating elements, spanning bands of the considered parameter space. After forming estimates of the initially activated bands, these are retained and refined, whereas non-activated bands are discarded from the further optimization, resulting in a smaller and zoomed dictionary with a finer grid. Implementing this scheme allows for reliable sparse signal reconstruction, at a much lower computational cost as compared to directly forming a larger dictionary spanning the whole parameter space. Simulation and real data processing results demonstrate that the proposed wideband estimator offers significant computational savings, without noticeable loss of performance.**

***Index Terms*— Generalized sparse reconstruction, covariance-based sparse estimation, scanning radar, wideband dictionary.**

I. Introduction

RECONSTRUCTING the fine details of the reflectivity function from a coarse scale measurement is a topic of notable relevance in a wide range of microwave sensing applications. It can provide improved resolution for various real aperture sensors, such as scanning radars, scatterometers, and radiometers [1]–[4]. The scanning radar is a kind of active microwave sensor that sweeps an antenna beam through the entire field of view to form the microwave image in azimuth direction. The received measurement in azimuth can thus be modeled as the result between the reflectivity function and the actual antenna pattern, such that the measured signal may be modeled as [1], [5]

$$\mathbf{y} = \mathbf{s} \star \mathbf{h} + \mathbf{n} \tag{1}$$

where $\star$ denotes the convolution operation, $\mathbf{y} \in \mathbb{C}^{M\times 1}$ the azimuth echo, $\mathbf{s} \in \mathbb{C}^{K\times 1}$ the reflectivity function, $\mathbf{h} \in \mathbb{C}^{L\times 1}$ the antenna pattern, and $\mathbf{n} \in \mathbb{C}^{M\times 1}$ an additive noise term. As may be seen from (1), the reflectivity function is smoothed by the antenna pattern, implying that the resolution of the azimuth echo is constrained by the antenna pattern. Early works interpret reconstructing the reflectivity function as solving a linear system of equations, such that [6]

$$\mathbf{y} = \mathbf{A}\mathbf{s} + \mathbf{n} \tag{2}$$

where $\mathbf{A} \in \mathbb{C}^{M\times K}$ is a typical circulant matrix, each column of which is the shifted version of the antenna pattern, $\mathbf{h}$. Because of the low-pass character of the antenna pattern, the linear inversion problem of determining $\mathbf{s}$ from (2) is generally ill-conditioned. As a result, multiple methods incorporating various regularization procedures have been developed over the past decades, including direct methods, such as inversion technique based on the Tikhonov regularization (REGU) [7], the truncated singular value decomposition (TSVD) approaches [4], [8], [9], as well as iterative methods, such as the iterative scatterometer image reconstruction (SIR) [10], [11] and the gradient methods [12], [13]. These methods have been shown to be able to well handle the ill-conditioned deconvolution problem and to decrease the noise amplification significantly. However, these advantages are achieved at the cost of limited resolution improvement.

Alternatively, reflectivity function reconstruction can be performed by inverse filtering in the frequency domain. The Fourier representation of (1) can be expressed as

$$\mathbf{Y} = \mathbf{S} \odot \mathbf{H} + \mathbf{N} \tag{3}$$

where $\odot$ denotes the Schur-Hadamard (element-wise) product, whereas $\mathbf{Y}$, $\mathbf{S}$, $\mathbf{H}$, and $\mathbf{N}$ denote the Fourier transforms of $\mathbf{y}$, $\mathbf{s}$, $\mathbf{h}$, and $\mathbf{n}$, respectively. Reconstructing the reflectivity function in the frequency domain can be formulated as the task of finding a linear operator $\mathbf{G}$, such that

$$\mathbf{S} = \mathbf{G} \odot \mathbf{Y} \tag{4}$$

In principle, the deconvolution of this operator can be formed by a direct inverse filter constructed as $\mathbf{G} = 1/\mathbf{H}$, with the division being formed element-wise. In this manner, the spectrum of the reflectivity function can be recovered as

$$\hat{\mathbf{S}}_{\mathrm{IF}} = \frac{\mathbf{Y}}{\mathbf{H}} \tag{5}$$

from which the desired reflectivity function may be determined as $\hat{\mathbf{s}}_{\mathrm{IF}} = \mathscr{F}^{-1}\left(\hat{\mathbf{S}}_{\mathrm{IF}}\right)$, where $\mathscr{F}^{-1}(\cdot)$ denotes the inverse Fourier transform. However, typical antenna patterns result in strong low-pass filtering. Therefore, high frequencies are filtered out and the elements in $1/\mathbf{H} \to \infty$ at high frequencies, resulting in a destructive noise amplification. One straightforward method to suppress this noise ampliation is using a

This work was supported by the National Natural Science Foundation of China under Grant 61671117, the Collaborative Innovation Center for Radar Technique of Ministry of Education of China, and the Swedish Research Council.

windowed inverse filter, resulting in the windowed spectrum

$$\mathbf{S}_{\mathrm{w}} = \mathbf{W}_N \odot \hat{\mathbf{S}}_{\mathrm{IF}} \tag{6}$$

where $\mathbf{W}_N \in \mathbb{C}^{M\times 1}$ denotes the used window, the width of which, N, should be smaller than the bandwidth of the antenna pattern. Because partial frequencies that are less reliable in $\hat{\mathbf{S}}_{\mathrm{IF}}$ are suppressed to zero, the degree of ill-conditioning resulting from inverse filtering can be decreased. However, the window $\mathbf{W}_N$ will aggravate the smoothing effect on the direct inverse filtering. One option is to use Wiener filtering, being constructed so that the expected value of the squared difference between the estimate and the true value is minimized [14], [15]. The limitation of Wiener filtering is the requirement for prior information on the covariance characteristic of the reflectivity function. Generally, this is not available for practical applications, resulting in that empirical assumptions must be added on the prior information when realizing the Wiener filter [15].

The problem of reconstructing the reflectivity function is equivalent to parameter estimation, where the major parameters include the amplitudes and the locations. Therefore, many statistical techniques with excellent performance and inherent robustness to the model assumptions presented for spectral estimation, such as the Capon beamformer, the multiple signal classification (MUSIC), and the amplitude and phase estimation (APES) algorithms, can be applied to scanning radar sensing [16]–[18]. Regrettably, these algorithms all require a large number of snapshots, as well as uncorrelated targets, conditions that are rarely satisfied in practical microwave sensing. In [19], [20], the iterative adaptive approach (IAA) and its regularized version were proposed, and were shown to overcome several of the drawbacks of conventional statistical methods for array processing. Given this, the IAA was recently formulated for scanning radar sensing, and was demonstrated to outperform the earlier mentioned methods, such as the REGU, TSVD, gradient methods, and Wiener filtering, in both resolution improvement and noise suppression [6], [21].

In some scanning radar applications, such as airport surveillance, harbour monitoring of aircrafts or vessels, and most surface-to-air problems, the number of targets in the reflectivity function is substantially lower than the number of potential source locations. Therefore, sparse reconstruction techniques can be used to provide significant sidelobe suppression and more accurate target descriptions. Sparse signal representation aims at minimizing $\|\mathbf{s}\|_0$, such that $\mathbf{y} = \mathbf{A}\mathbf{s}$ is satisfied [22]. However, minimizing $\|\mathbf{s}\|_0$ quickly results in an infeasible combinatorial problem. Many classical sparse methods, such as the least absolute shrinkage and selection operator (LASSO) [23], focal underdetermined system solution (FOCUSS) [24], and sparse Bayesian learning (SBL) [25] have focused on formulating convex algorithms that instead exploit different sparsity inducing penalties on $\|\mathbf{s}\|_1$. The potential drawback of the LASSO and FOCUSS is the selection of one or more hyperparameters, which relies on prior knowledge of $\mathbf{s}$. The SBL does not require such hyperparameters, but it converges quite slowly. In [19], the IAA algorithm was extended with the Bayesian information criterion (BIC) to provide sparse estimation, and further improve the result of the relaxation-based cyclic approach (RELAX). This IAA-APES&RELAX algorithm was shown to provide better variance and bias characteristics than other examined methods, and result in lower computational complexity. Moreover, the method does not require any hyperparameter. In [26], the Sparse Learning via Iterative Minimization (SLIM) method was developed for multiple-input multiple-output (MIMO) radar. It was there shown to require a notably lower computational burden than the IAA-APES&RELAX algorithm. In addition, it was shown to offer more accurate estimates as compared to the widely-used CoSaMP approach. In [27], a novel sparse method, termed the SParse Iterative Covariance-based Estimation (SPICE) algorithm was proposed based on a covariance fitting criteria. The SPICE algorithm is globally convergent, and does not require any choice of user parameter. Moreover, it was also demonstrated to provide more accurate estimates as compared to SLIM. However, it incorporates a 1-norm penalty (sparse constraint) on both the signal and the noise components simultaneously, and may thus strive to reduce the noise powers rather than the signal components. As a result, one may obtain a singular, or at least a poorly conditioned covariance matrix. In order to avoid this problem, the q-SPICE algorithm was developed by generalizing the formulation to allow for a varying q-norm constraint on the noise for $q \geq 1$ [28], which was shown to yield more accurate estimates when compared with the SPICE estimates.

Recently, the q-SPICE algorithm was extended to scanning radar applications and was there shown to outperform the IAA [29]. In this paper, we further this development on sparse reconstruction in scanning radar applications using the q-SPICE method. The early work on using q-SPICE in scanning radar applications was developed in the time domain. This formulation suffers from numerical unreliability because the dictionary $\mathbf{A}$ may be rank-deficient, although some adaptive regularization was made to allow for this in the q-SPICE formulation. To overcome this drawback, we here develop the q-SPICE algorithm in the frequency domain. The frequency-domain signal model comes from the windowed inverse filtering in (6), where the frequency-domain dictionary is typically consistent with that of spectral analysis applications. Therefore, the q-SPICE implementation in the frequency domain inherits the numerical reliability observed in [28].

Like many other sparse algorithms, the q-SPICE method requires the computation of the covariance matrix, its inverse, and the resulting estimate for each sampling grid point. This generally results in a notable computational burden, especially when this estimator is formed over a fine dictionary. Based on the inherent Fourier structure of the dictionary and the Toeplitz structure of the covariance matrix, it may be noted that earlier fast methods developed for the IAA algorithm [30]–[37] would also be applicable to a similar implementation of the q-SPICE method. Such an implementation is clearly feasible, and one may achieve notable computational reduction by efficiently computing the covariance matrix in a way of fast Fourier transform (FFT) and fast solving of the Toeplitz equation system via an appropriate Gohberg-Semencul representation. However, such an implementation will still neglect the inherent sparseness of the target distribution. Because only a finite

number of targets contribute to the covariance matrix, it is not necessary to form the estimates for the entire parameter space as most elements of the reflectivity function will be zero, or close to zero. Motivated by the need to reduce the computational complexity, exploiting the ideas introduced in [38] for the LASSO, we here develop a wideband q-SPICE method by integrating the dictionary over several bands of the parameter space. Using an initial wideband dictionary with a coarse grid, the bands that cover the true targets can be activated efficiently. In the subsequent screening procedure, the activated bands are then retained and refined, whereas any non-activated bands are discarded, resulting in a smaller and zoomed dictionary with finer grid. Because the dimension of the parameter space is reduced in the zoomed dictionary, the wideband q-SPICE method will enjoy lower computational complexity. Meanwhile, the contribution from true targets are still retained, and the grid size of the zoomed dictionary can be set to any desired resolution, so the wideband q-SPICE method will not suffer noticeable performance degradation as compared to its narrowband implementation. Moreover, as the covariance matrix formed by the refined dictionary in the screening procedure maintains the Toeplitz structure, the computational cost of the wideband q-SPICE method may be further reduced by exploiting the inherent structure of the estimator, reminiscent of the implementation derived for the IAA algorithm.

The remaining parts of this paper are organized as follows: in section II, we introduce the signal reconstruction model for scanning radar in the frequency domain. In section III, the wideband q-SPICE algorithm is detailed. In section IV and V, the simulation and real data processing results are presented to demonstrate the improvement on computational efficiency of the proposed method. Finally, conclusions are provided in section VI.

II. Frequency-domain Signal Model

For practical applications, Fourier transforms are calculated by the discrete Fourier transform (DFT). Therefore, we consider discrete frequencies varying from 0 to 2π. Let $\widehat{\mathbf{u}}$ denote the vector obtained by swapping the up and down halves of a vector $\mathbf{u}$, and $\tilde{\mathbf{u}}$ denote the vector obtained by flipping a vector $\mathbf{u}$ in the up/down direction.

Furthermore, let $\mathbf{W}_N$ denote the rectangular window, whereas $\mathbf{z} \in \mathbb{C}^{N\times 1}$ and $\mathbf{e} \in \mathbb{C}^{N\times 1}$ denote the vectors that include the non-zero elements truncated from $\widehat{\mathbf{S}}_{\mathrm{w}}$ and $\mathbf{W}_N \odot \left(\widehat{\mathbf{N}}/\widehat{\mathbf{H}}\right)$, respectively. Let

$$\mathbf{F} = [\mathbf{f}_1, \mathbf{f}_2, \ldots, \mathbf{f}_M] \tag{7}$$

denote the $N \times M$ Fourier matrix with

$$\mathbf{f}_m = \left[1, \mathrm{e}^{j\omega_m}, \ldots, \mathrm{e}^{j\omega_m(N-1)}\right]^{\mathrm{T}} \tag{8}$$

$$\omega_m = \frac{2\pi}{M}(m-1) \tag{9}$$

for $m = 1, \ldots, M$, where $(\cdot)^{\mathrm{T}}$ denotes the transpose, and the $M \times 1$ vector

$$\boldsymbol{\alpha} = \begin{bmatrix} \mathbf{s} \\ \mathbf{0} \end{bmatrix} \odot \boldsymbol{\varphi}(\omega) \tag{10}$$

with

$$\boldsymbol{\varphi}(\omega) = \left[\mathrm{e}^{-j\omega_0(N/2)}, \mathrm{e}^{-j\omega_1(N/2)}, \ldots, \mathrm{e}^{-j\omega_{M-1}(N/2)}\right]^{\mathrm{T}} \tag{11}$$

Then, the relationship between the flipped version of $\mathbf{z}$ and $\mathbf{s}$ may be expressed as (see also [5])

$$\tilde{\mathbf{z}} = \mathbf{F}\boldsymbol{\alpha} + \tilde{\mathbf{e}} \tag{12}$$

Thus, if $\boldsymbol{\alpha}$ can be estimated, the reflectivity function $\mathbf{s}$ may be recovered via (10). This is the so-called frequency-domain signal model for scanning radar in the azimuth direction. Unlike the dictionary $\mathbf{A}$ with the circulant structure in (2), the dictionary $\mathbf{F}$ is a Fourier matrix. This makes the reconstruction methods using $\mathbf{F}$ inherit the numerical stability often found in spectral analysis applications.

The frequency-domain model introduces a user parameter, N. From the view of resolution improvement and sidelobe rejection, a larger window width, N, is preferred as a smaller N would aggravate the smoothing effect and decrease the degrees of freedom. However, N also influences the signal-to-noise ratio (SNR) in the frequency domain. A detailed analysis of this effect depends on the types of the noise and the antenna pattern, $\mathbf{h}$. In scanning radar applications, the noise can typically be well modeled as an additive white Gaussian noise (AWGN), whereas the two-way antenna pattern, $\mathbf{h}$, is often expressed using the square Sinc type [39]. In the case of AWGN, the noise spectrum is uniform at all frequencies, whereas the spectrum of the two-way antenna pattern is the triangle function. Therefore, a smaller N is preferred as the noise will be suppressed less at frequencies close to zero. Under the assumptions of AWGN and using a square Sinc type antenna pattern, the width N of the window $\mathbf{W}_N$ therefore has the role of a regularization parameter, and balances the trade-off between noise amplification and resolution improvement. This follows the property of the regularization parameter in existing reconstruction approaches.

III. The Wideband q-SPICE algorithm

The model (12) allows for applying various spectral analysis methods to recover the reflectivity function. The recent SPICE algorithm is globally convergent, and does not require any choice of user parameter. Moreover, it has been demonstrated to provide more accurate estimates than other popular methods, such as the SLIM and IAA algorithms for sparse signal reconstruction [27], [40].

A. SPICE

Assuming that the measured noise is uncorrelated over the measurement, the noise covariance matrix may be expressed as

$$\mathrm{E}\left(\tilde{\mathbf{e}}\tilde{\mathbf{e}}^{\mathrm{H}}\right) = \mathrm{diag}\left(\left[\sigma_1^2, \sigma_2^2, \ldots, \sigma_N^2\right]\right) \tag{13}$$

where $\mathrm{E}(\cdot)$ denotes the expectation, $(\cdot)^{\mathrm{H}}$ the conjugate transpose, and $\mathrm{diag}(\cdot)$ a diagonal matrix formed from the specified vector. Thus, the covariance matrix of $\tilde{\mathbf{z}}$ may be expressed as

$$\begin{aligned}\mathbf{R} = \mathrm{E}\left(\tilde{\mathbf{z}}\tilde{\mathbf{z}}^{\mathrm{H}}\right) &= \sum_{m=1}^{M} |\alpha_m|^2 \mathbf{f}_m \mathbf{f}_m^{\mathrm{H}} + \mathrm{E}\left(\tilde{\mathbf{e}}\tilde{\mathbf{e}}^{\mathrm{H}}\right) \\ &\triangleq \mathbf{B}\mathbf{P}\mathbf{B}^{\mathrm{H}}\end{aligned} \tag{14}$$

where

$$\boldsymbol{\alpha} \triangleq [\alpha_1, \alpha_2, \ldots, \alpha_M]^{\mathrm{T}} \tag{15}$$

$$\mathbf{B} = \begin{bmatrix} \mathbf{F} & \mathbf{I} \end{bmatrix} \triangleq [\mathbf{b}_1, \mathbf{b}_2, \ldots, \mathbf{b}_{M+N}] \tag{16}$$

$$\begin{aligned} \mathbf{P} &= \mathrm{diag}\left(\left[|\alpha_1|^2, |\alpha_2|^2, \ldots, |\alpha_M|^2, \sigma_1^2, \sigma_2^2, \ldots, \sigma_N^2\right]\right) \\ &\triangleq \mathrm{diag}\left([p_1, p_2, \ldots, p_{M+N}]\right) \\ &\triangleq \mathrm{diag}\left(\mathbf{p}\right) \end{aligned} \tag{17}$$

with $\mathbf{I}$ denoting the $N \times N$ identity matrix. In order to estimate $\boldsymbol{\alpha}$, one may define the weighted covariance fitting criterion (see also [27])

$$f = \left\| \mathbf{R}^{-1/2} \left(\tilde{\mathbf{z}}\tilde{\mathbf{z}}^{\mathrm{H}} - \mathbf{R} \right) \right\|_{\mathrm{F}}^2 \tag{18}$$

where $\|\cdot\|_{\mathrm{F}}$ denotes the Frobenius norm, and $\mathbf{R}^{-1/2}$ the Hermitian positive definite square root of $\mathbf{R}^{-1}$. As shown in [27], minimizing (18) is equivalent to

$$\min_{\{p_m \geq 0\}} \ \tilde{\mathbf{z}}^{\mathrm{H}} \mathbf{R}^{-1} \tilde{\mathbf{z}} + \|\mathbf{W}\mathbf{p}\|_1 \tag{19}$$

where $\|\cdot\|_1$ denotes the 1-norm, and

$$w_m = \frac{\|\mathbf{b}_m\|^2}{\|\tilde{\mathbf{z}}\|^2}, m = 1, 2, \ldots M + N \tag{20}$$

$$\mathbf{W} = \mathrm{diag}\left([w_1, w_2, \ldots, w_{M+N}]\right) \tag{21}$$

The formulation thus minimizes a signal fitting criteria, which measures the distance through the inverse of the (model) covariance matrix. The minimization in (19) is a convex semidefinite program, which may be solved using standard convex solvers, although a direct minimization is typically computationally cumbersome. To allow for a more efficient solution, (19) may be rewritten to the equivalent constrained minimization problem [27]

$$\min_{\{p_m \geq 0\}} \ \tilde{\mathbf{z}}^{\mathrm{H}} \mathbf{R} \tilde{\mathbf{z}} \ \text{ s.t. } \|\mathbf{W}\mathbf{p}\|_1 = 1 \tag{22}$$

which may be solved efficiently by iterating

$$\rho\left(i\right) = \sum_{m=1}^{N+M} w_m^{1/2} p_m\left(i\right) \left|\mathbf{b}_m^{\mathrm{H}} \mathbf{R}^{-1}\left(i\right) \tilde{\mathbf{z}}\right| \tag{23}$$

$$p_m\left(i+1\right) = p_m\left(i\right) \frac{\left|\mathbf{b}_m^{\mathrm{H}} \mathbf{R}^{-1}\left(i\right) \tilde{\mathbf{z}}\right|}{w_m^{1/2} \rho\left(i\right)} \tag{24}$$

with the initialization

$$p_m\left(0\right) = \frac{\left|\mathbf{b}_m^{\mathrm{H}} \tilde{\mathbf{z}}\right|^2}{\left|\mathbf{b}_m^{\mathrm{H}} \mathbf{b}\right|^2} \tag{25}$$

where i is the iteration number. Once p_m, for $m = 1, \ldots, M$, is estimated, the reflectivity function $\mathbf{s}$ can be therefore reconstructed from (10), (17), and (24).

It is worth noting that the constraint in (22) is a weighted 1-norm. Therefore, a sparse solution can be obtained by the SPICE algorithm. However, this constraint does not distinguish the signal and noise components, and as a result, some estimates of the σ_n^2 may be forced to be zero as a part of the minimization. As one is typically interested in finding a sparse solution from the columns of the dictionary $\mathbf{F}$, it make no sense to set some of the noise parameters σ_n^2 to zero, and may even lead $\mathbf{R}$ to lose rank or become poorly conditioned.

B. q-SPICE

The q-SPICE formulation strives to address this problem by reformulating the criterion in (19) as [28]

$$g = \tilde{\mathbf{z}}^{\mathrm{H}} \mathbf{R}^{-1} \tilde{\mathbf{z}} + \|\mathbf{W}_{\mathrm{s}} \mathbf{p}_{\mathrm{s}}\|_1 + \|\mathbf{W}_{\mathrm{n}} \mathbf{p}_{\mathrm{n}}\|_q \tag{26}$$

where

$$\mathbf{p}_{\mathrm{s}} = [p_1, p_2, \ldots, p_M]^{\mathrm{T}} \tag{27}$$

$$\mathbf{p}_{\mathrm{n}} = [p_{M+1}, p_{M+2}, \ldots, p_{M+N}]^{\mathrm{T}} \tag{28}$$

$$\mathbf{W}_{\mathrm{s}} = \mathrm{diag}\left([w_1, w_2, \ldots, w_M]\right) \tag{29}$$

$$\mathbf{W}_{\mathrm{n}} = \mathrm{diag}\left([w_{M+1}, w_{M+2}, \ldots, w_{M+N}]\right) \tag{30}$$

with $\|\cdot\|_q$ denoting the q-norm, with $q \geq 1$. Thus, the original SPICE formulation is obtained for the case when $q = 1$. Defining

$$\boldsymbol{\beta} = \mathbf{P}\mathbf{B}^{\mathrm{H}} \mathbf{R}^{-1} \tilde{\mathbf{z}} \triangleq \left(\beta_1, \beta_2, \ldots, \beta_{M+N}\right)^{\mathrm{T}} \tag{31}$$

the minimizing of (26) may be formed by iteratively computing [28]

$$\lambda = \left(\left\| \mathbf{W}_{\mathrm{s}}^{1/2} \boldsymbol{\beta}_{\mathrm{s}} \right\|_1 + \left\| \mathbf{W}_{\mathrm{n}}^{1/2} \boldsymbol{\beta}_{\mathrm{n}} \right\|_{\frac{2q}{q+1}} \right)^2 \tag{32}$$

$$p_m = \begin{cases} \dfrac{|\beta_m|}{\sqrt{w_m} \lambda^{1/2}}, m = 1, 2, \ldots, M \\ \dfrac{|\beta_m|^{\frac{2}{q+1}} \left\| \mathbf{W}_{\mathrm{n}}^{1/2} \beta_{\mathrm{n}} \right\|^{\frac{q-1}{q+1}}_{\frac{2q}{q+1}}}{w_m^{\frac{q}{q+1}} \lambda^{1/2}}, m = M+1, \ldots, M+N \end{cases} \tag{33}$$

where

$$\boldsymbol{\beta}_{\mathrm{s}} = [\beta_1, \beta_2, \ldots, \beta_M]^{\mathrm{T}} \tag{34}$$

$$\boldsymbol{\beta}_{\mathrm{n}} = [\beta_{M+1}, \ldots, \beta_{M+N}]^{\mathrm{T}} \tag{35}$$

These iterations can also be initiated using (25). Compared with the SPICE algorithm, the q-SPICE algorithm considers the signal and noise terms separately, as shown by (26). The q-norm penalty on the noise makes a dense estimate on the noise variance, which results in that $\mathbf{R}$ will be full rank. The influence of the selection of q was investigated in [28], where $1 < q < 2$ was shown to yield preferable solutions, resulting in more accurate estimation. For larger values of q ($q > 3$), it was also observed that q-SPICE may suffer from the risk of target loss.

C. Wideband q-SPICE

The main computational burden of q-SPICE results from forming $\mathbf{R}$ with (14) and the computation of (31), resulting in a computational complexity of $\mathcal{O}\left(MN^2 + N^3\right)$ for each iteration.

With the prior knowledge of the sparseness of the signal of interest, only a finite number of targets will contribute to $\mathbf{R}$. In addition, it is not necessary to form the estimates for all sampling grid points as most of these elements will be zero. To reduce the computational redundancy, one may

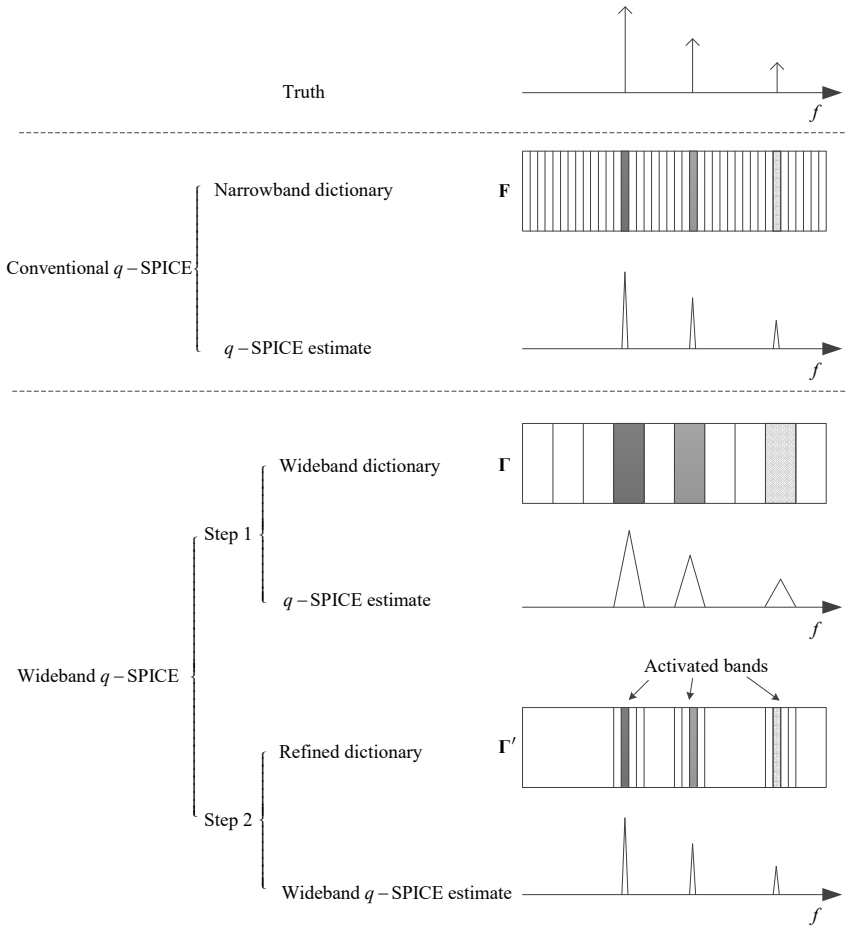

Fig. 1. Schematic diagram of the noise-free wideband q-SPICE method.

instead proceed to use a wideband dictionary, $\mathbf{\Gamma}$, over $B < M$ frequency bands. Define

$$\omega'_b = \frac{2\pi}{B}(b-1) \tag{36}$$

for $b = 1, \ldots, B+1$. Then, the element at the nth row and bth column of $\mathbf{\Gamma}$ is formed as

$$\begin{aligned}\mathbf{\Gamma}_{n,b} &= \frac{1}{2\pi}\int_{\omega'_b}^{\omega'_{b+1}} \mathrm{e}^{j\omega(n-1)}\mathrm{d}\omega \\ &= \begin{cases} \dfrac{1}{B}, & n = 1 \\ \dfrac{\mathrm{e}^{j\omega'_{b+1}(n-1)} - \mathrm{e}^{j\omega'_b(n-1)}}{j2\pi(n-1)}, & 1 < n \leq N \end{cases}\end{aligned} \tag{37}$$

Using the wideband dictionary $\mathbf{\Gamma}$ instead of $\mathbf{F}$, and following the iterative procedures in (32) and (33), it is possible to activate the bands that cover the true targets with the q-SPICE algorithm much more efficiently since $B < M$. To activate the bands, we thus retain only the bands with significant power above an empirical threshold τ. Furthermore, the activated bands are refined with a fine grid size, which is the same as that of the conventional dictionary, $\mathbf{F}$, and form the refined bands as another dictionary, $\mathbf{\Gamma}'$. Then, we use $\mathbf{\Gamma}'$ instead of $\mathbf{F}$, and following the iterative procedures in (32) and (33) to reconstruct $\mathbf{s}$ without loss of resolution. For example, when $M = 1000$, the frequency grid size of $\mathbf{F}$ is 0.002π. We may then use $B = 20$ bands, and refine each activated bands with $Q = 50$ sampling points. Then, the grid size of $\mathbf{\Gamma}'$ is 0.002π and is consistent with that of $\mathbf{F}$. Clearly, one may also choose to further refine the estimate by increasing the number of zooming steps forward. The schematic diagram of the wideband q-SPICE is illustrated in Fig.1.

Because many non-activated bands have been discarded, the dimension of the parameter space is reduced in the zoomed dictionary $\mathbf{\Gamma}'$. The wideband q-SPICE will thus enjoy lower computational complexity. Although the wideband q-SPICE contains two steps of the q-SPICE implementation, the total computational complexity is smaller than that of the conventional q-SPICE implementation.

IV. Simulation results

Scanning radar forms 2-D image estimates by transmitting linear frequency-modulated (LFM) pulses at a given pulse repetition frequency (PRF), and circularly sweeping a narrow beam through the entire field of view. We generate the simulated raw echo according to this process. It is known that the number of sampling points in azimuth may be formed as [5]

$$M = \frac{\Phi}{\Omega}\mathrm{PRF} \tag{38}$$

where Φ is the azimuth scope and Ω is the scanning speed. In range, the echo is first processed by matched filtering

TABLE I
SIMULATION PARAMETERS

Parameter	Value
Bandwidth	60 MHz
Pulse width	2 μs
Scanning velocity	$60^\circ/s$
Beamwidth	3°
Sampling rate	80 MHz

to enhance the range resolution and the SNR simultaneously. Then, we proceed to process the echo further with the discussed reconstruction methods in azimuth. The main simulation parameters are shown in Table I.

The targets of interest and the radar platform are here assumed to be stationary. Furthermore, an ideal $(\sin x/x)^2$ antenna pattern is adopted in our simulations, of which we only consider the mainlobe, as shown in Fig.2(a). For all approaches considered, the scanning grid is uniform in azimuth. Here, we consider the AWGN, with the SNR defined as

$$\text{SNR} = 10\log_{10}\frac{P_s}{\sigma^2} \tag{39}$$

where P_s is the peak power of the raw echo. We proceed to investigate the performance of the IAA [19], the regularized IAA (IAA-R) [20], the SLIM [26], as well as the discussed various versions of the SPICE algorithm. The used stopping criterion is set as

$$\|\hat{\mathbf{s}}_i - \hat{\mathbf{s}}_{i-1}\|_2 < 10^{-3} \tag{40}$$

where $\hat{\mathbf{s}}_i$ is the reconstructed result at the ith iteration.

A. Reconstruction result comparison

The number of sampling points within the bandwith of the antenna pattern is approximately $N_B = 10$. We set the width of the window $\mathbf{W}_N$ to $N = 9$, considering the noise suppression and smoothing effect for all methods.

To compare the reconstruction results for the proposed and the existing methods, we form a synthetic field as shown in Fig.2(b), where several groups of adjacent sparse targets with varying space are set in different range cells. Here, we set PRF to 4000 Hz, so that the number of azimuth sampling points is $M = 1200$. The range then covers from 3000 m to 3500 m from the sensor, with the azimuth range covering the targets from -9° to 9°, resulting in images of size 400×1200 (range $\times$ azimuth).

Fig.2(c) shows the raw echo obtained by the scanning radar with SNR = 10 dB. The targets are smoothed by the LFM pulses and the antenna pattern in range and azimuth, respectively. As a result, the raw echo suffers from the observed coarse resolution. Fig.2(d) presents the result after matched filtering in range. The resolution in range and the SNR has been improved significantly. However, the azimuth resolution is still low. As observed in Fig.2(e) and Fig.2(f), the IAA and IAA-R algorithms can successfully resolve all targets, but suffers from high sidelobes. The SLIM algorithm can reject the sidelobes better, as shown in Fig.2(g). By contrast, the SPICE method can well resolve all targets with much lower sidelobes, and the results are more sparse than those of the IAA, IAA-R, and SLIM estimates, as shown in Fig.2(h). However, some artifact occurs in the results. The q-SPICE and wideband q-SPICE methods can well reject these artifacts, as shown in Fig.2(i) and Fig.2(j). To further investigate the resolution improvement, the profiles of the azimuth cut located at the range cell of 3200 m extracted from Fig.2 are shown in Fig.3. The results of various methods are plotted in two subgraphs separately to be shown clearly. It is apparent that the q-SPICE and wideband q-SPICE methods result in a higher resolution, lower sidelobes, as well as better artifact rejection.

When the sampling grid does not cover the entire range of frequencies (from 0 to 2π), the covariance matrix iteratively estimated by the IAA may not be invertible or may suffer from a large condition number. This may result in that the IAA amplifies the noise and produces large estimation errors. By introducing the noise terms into the iteratively reformulated covariance matrix, the IAA-R often yields a more robust estimate with lower estimation error as compared with the IAA [20]. In this paper, because all frequencies are considered, the conditioning problem of the IAA is not significant and the improvement of the IAA-R is thus not noticeable, as shown by Fig.2(e), Fig.2(f), Fig.3(a), and Fig.6.

B. Computational time analysis

The q-SPICE estimate requires a computational time of about 38.9 seconds to form Fig.2(i). If implemented using the wideband q-SPICE with $B = 40$ bands, and $Q = 30$ sampling points for each activated band to achieve the same resolution, this reduces to 2.4 seconds to obtain Fig.2(j).

Using the measurements as shown by Fig.2(d), Fig.4 illustrates the computational time of the wideband q-SPICE for varying B. It is clear that the use of a very low or very large number of bands, B, will increase the computational burden of the wideband q-SPICE, but also that the method will be computationally preferable as compared to the regular q-SPICE estimates for all choices of $B > 1$. From the figure, the wideband q-SPICE is seen to perform most efficient when B is around $\sqrt{M} \approx 35$.

Next, we change the parameter PRF and get the measurements with varying M in azimuth. Fig.5 shows the computational times of the wideband q-SPICE, for varying M. For each case of M, we select B as the integer nearest to $\sqrt{M}$. As observed in Fig.5, with the increasing M, the improvement of computational efficiency of the wideband q-SPICE becomes more prominent.

C. Mean squared error (MSE) comparison

We proceed to define the angular MSE as

$$\text{MSE} = \frac{1}{X}\sum_{x=1}^{X}(\hat{\mu}_x - \mu)^2 \tag{41}$$

where μ is the true angular parameter, $\hat{\mu}_x$ is the estimation of μ at the $x\text{th}$ trial, and X is the total number of Monte-Carlo trials. In this sub-section, 500 Monte-Carol trials was used to calculate the angular MSE.

One target is placed at 0°, using a PRF of 4000 Hz. To calculate the MSE, we consider the signals with the largest

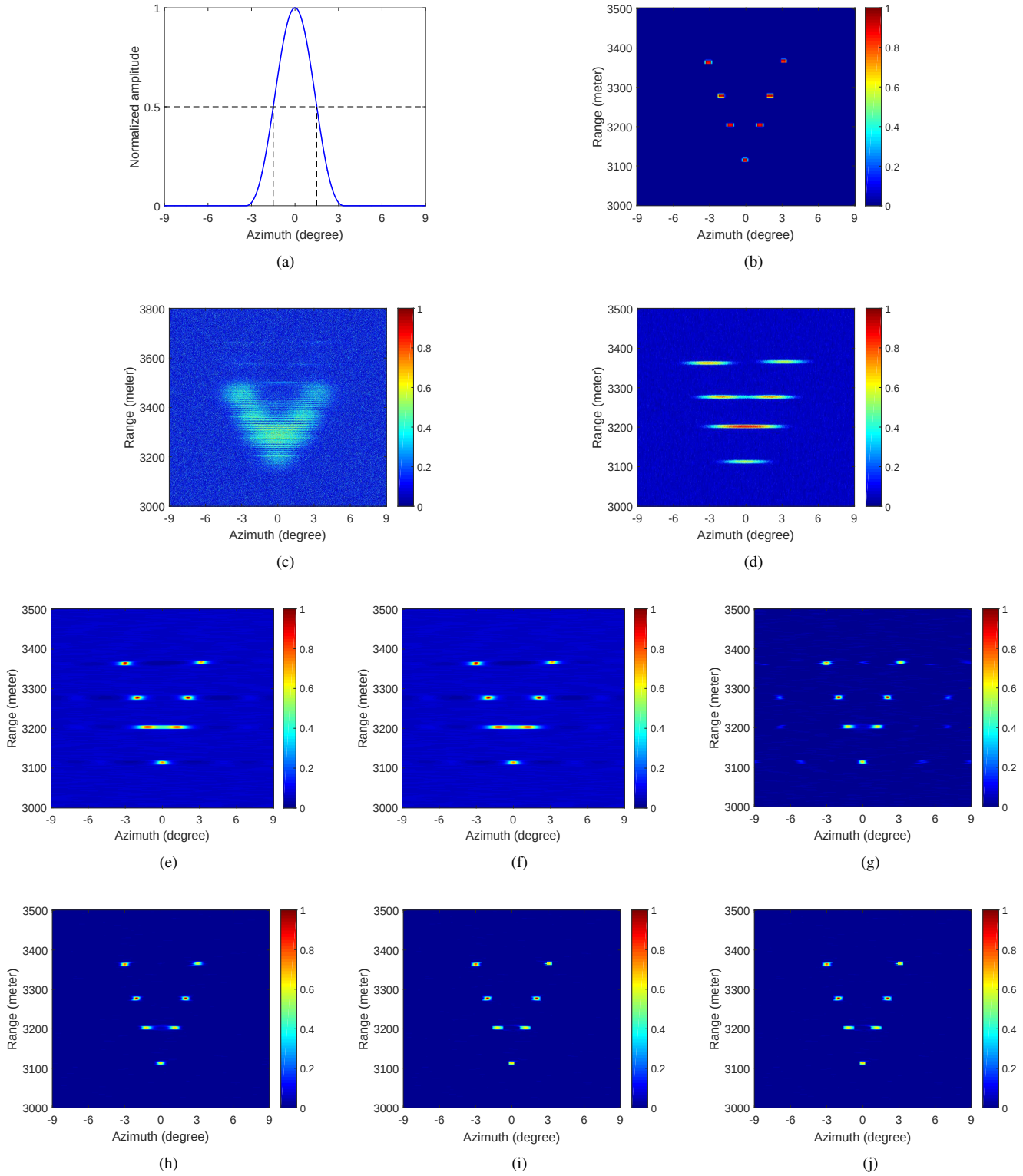

Fig. 2. Reconstruction result comparison for varying approaches. (a) Antenna pattern. (b) Truth. (c) Raw echo with SNR = 10 dB. (d) Result of match filtering with improved range resolution and SNR. (e) Reconstruction with the IAA algorithm. (f) Reconstruction with the IAA-R algorithm. (g) Reconstruction with the SLIM algorithm. (h) Reconstruction with the SPICE algorithm. (i) Reconstruction with the q-SPICE algorithm for $q = 1.7$. (j) Reconstruction with the wideband q-SPICE algorithm for $q = 1.7$.

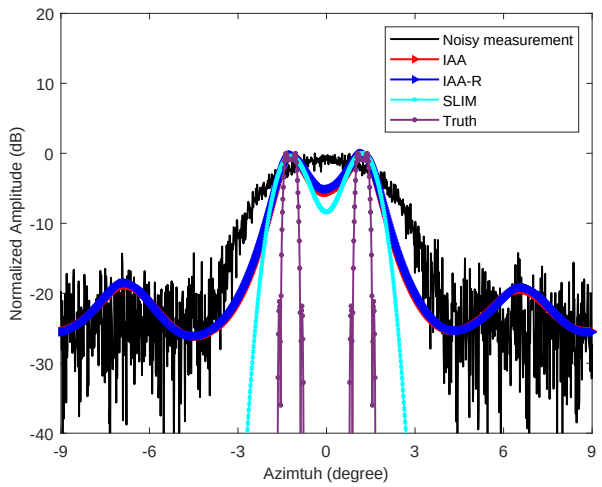

(a)

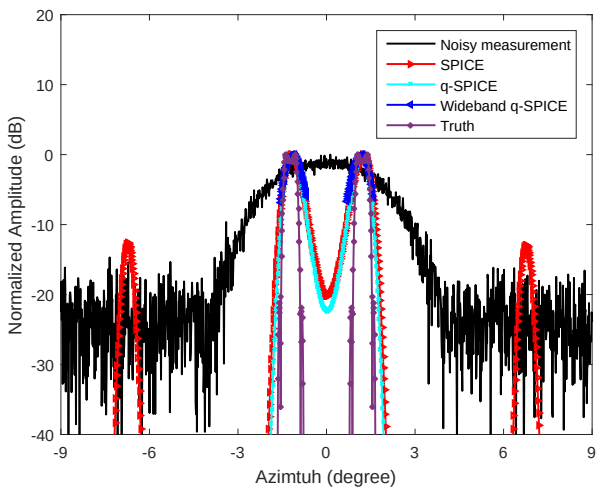

(b)

Fig. 3. Horizontal cuts extracted from Fig.2.

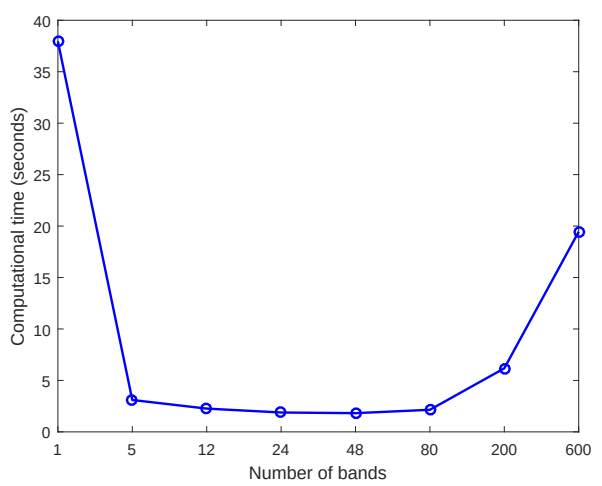

Fig. 4. Computational times of the wideband q-SPICE for varying B, when $M = 1200$.

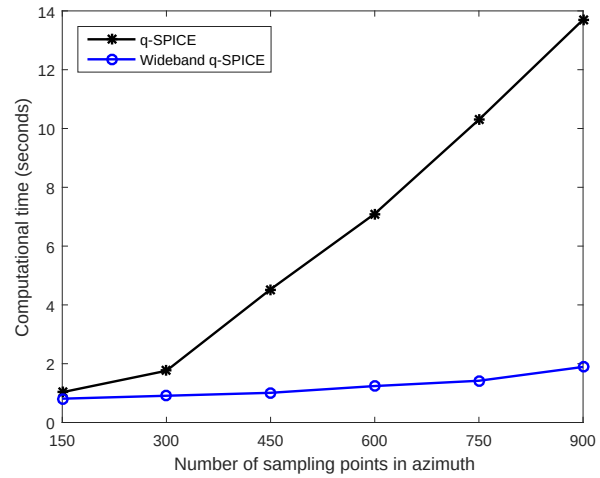

Fig. 5. Comparison of computational times between the q-SPICE and the wideband q-SPICE for varying number of sampling points in azimuth.

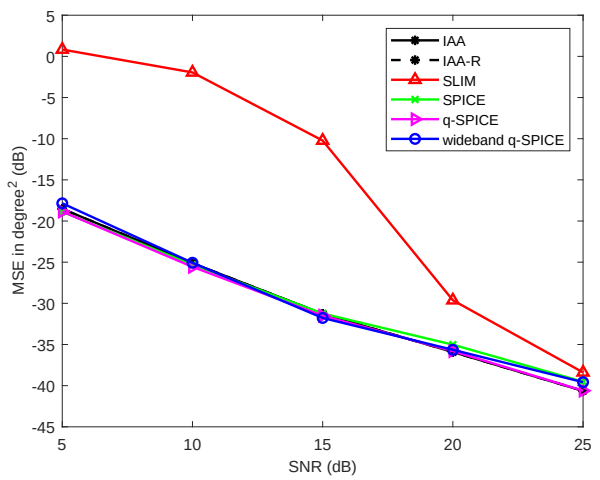

Fig. 6. Comparison of the MSE for varying methods.

peaks. Fig.6 compares the MSE of the angular estimates of each algorithm for varying SNR. We observe that all versions of SPICE have better variance characteristics than the SLIM, and have comparable variance characteristics to that of the IAA and IAA-R algorithms. Among all the versions of the SPICE, the q-SPICE method performs better than the conventional SPICE. This conclusion is consistent with that in [28]. The proposed wideband q-SPICE method achieves nearly the same performance as the q-SPICE method with a slight performance loss.

V. Real Data Processing

The previous analysis is based on simulation results, where the truth is ideally sparse. In practical applications, the ground truth is not strictly sparse because of the presence of clutter. In this section, we further demonstrate the performance of the wideband q-SPICE algorithm for real data case, where the truth contains both targets and background clutters. It is shown that the wideband q-SPICE algorithm can provide

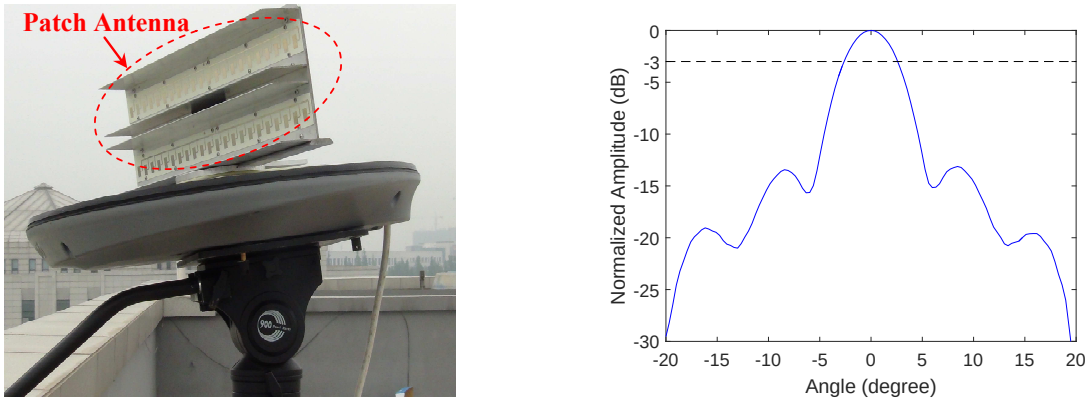

(a) (b)

Fig. 7. Radar system. (a) The X-band FMCW radar with a patch antenna. (b) Antenna pattern in azimuth.

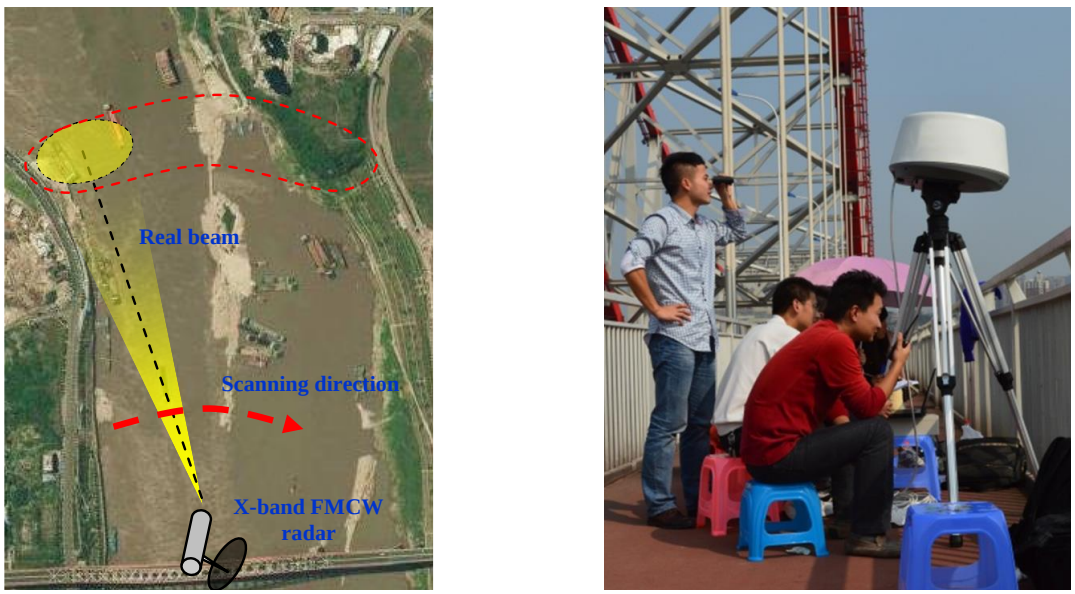

(a) (b)

Fig. 8. Experiment taken on a stationary platform. (a) Imaging mode. (b) Experimental site.

sparse reconstruction on the sparse targets, while suppressing the clutters well.

A. Radar System

The system is a wideband frequency modulated continuous wave (FMCW) radar operating at 9.4 GHz (X band), which provides a resolution of 2.6 meter and maximum 3700 meter coverage in range. It consists of one patch antenna shown by Fig.7(a), which generates the antenna beam with azimuth mainlobe width 5.1°, as shown by Fig.7(b). The mechanical servo allows for sweeping the antenna beam through the entire field of view within the range of 360 degrees. All the radar images will be displayed in a form of plan position indicators (PPIs).

B. Ground-based monitoring

Scanning radar is widely applied in various monitoring applications on a stationary platform in all-day and all-weather condition. For example, a shore-based scanning radar can be applied in a harbour for monitoring and searching for the illegal vessels. Similarly, an airport monitoring radar can track aircrafts and improve the safety of the flight. Here, we examine the ground-based monitoring problem, using an experiment at the Chaotianmen bridge, Chongqing. The radar sweeps the region with flight scanning speed of $72^\circ/s$ with a PRF of 200 Hz from -45° to 45°. The imaging mode and experimental site are shown in Fig.8.

There are several groups of boats on the Changjiang River. We first focus on the boats marked with the red circles in the optical scenario, as shown by Fig.9(a). The two boats are located close to each other, and they cannot be distinguished from the real beam data, as Fig.9(b) shows. The figures shown from Fig.9(c) to Fig.9(f) are the results of the IAA, IAA-R, q-SPICE, and the wideband q-SPICE approaches, respectively. As seen, the two boats can be resolved by all the

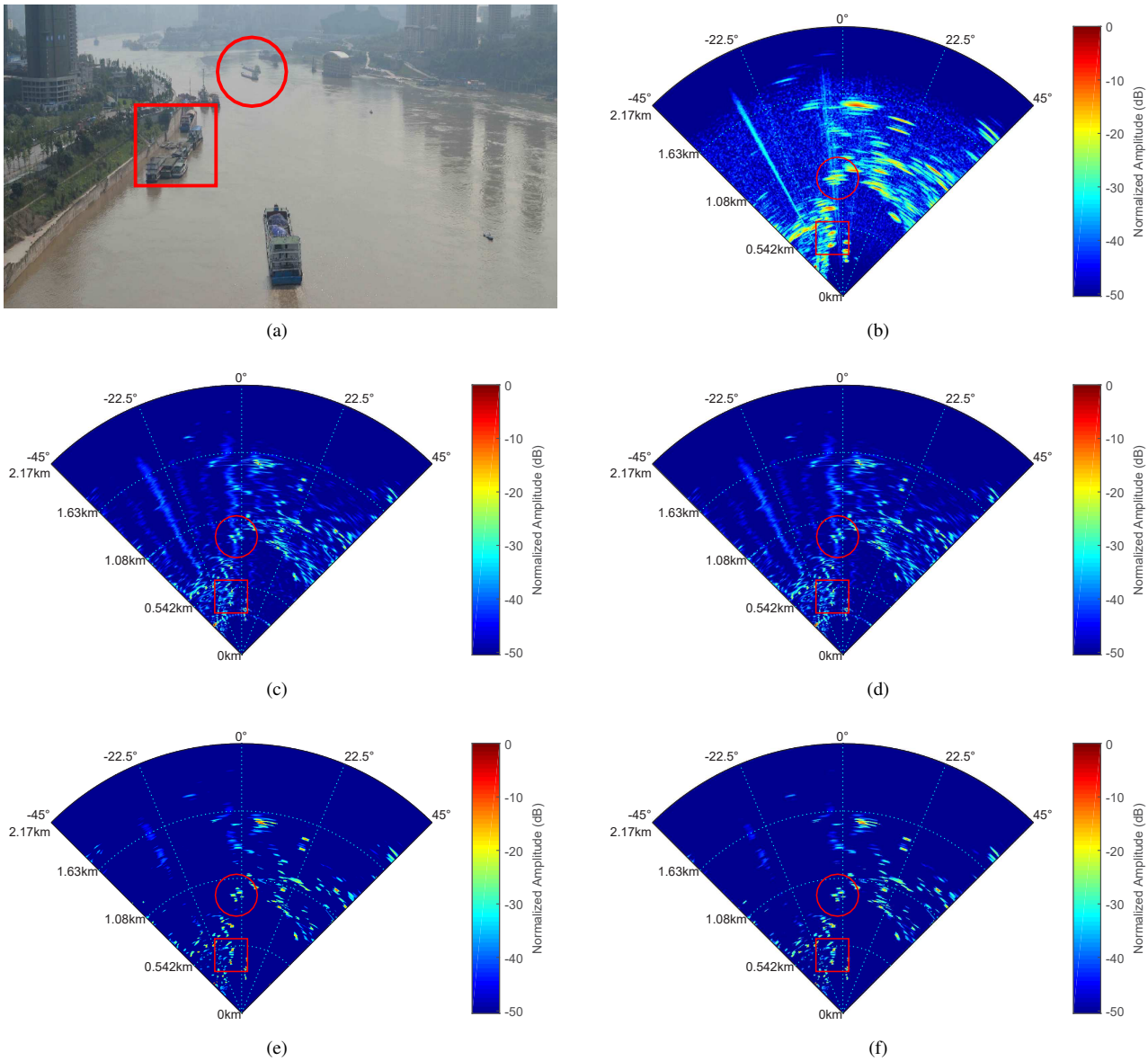

Fig. 9. Experiment taken on a stationary platform. (a) Optical scenario. (b) Real beam image after matched filtering in range. (c) Reconstruction result with the IAA. (d) Reconstruction result with the IAA-R.(e) Reconstruction result with the q-SPICE method ($q = 1.7$). (f) Reconstruction with the wideband q-SPICE method ($q = 1.7$).

methods, but the q-SPICE and wideband q-SPICE approaches result in lower sidelobes. This improvement can be further demonstrated by the results of the boats marked with the red boxes. Because the IAA and IAA-R suffer from higher sidelobes, the shore and boats cannot be resolved completely, as shown in Fig.9(c) and Fig.9(d). In contrast, the q-SPICE and wideband q-SPICE approaches can suppress the sidelobes and provide higher resolution. The shore and boats may be resolved, as seen in Fig.9(e) and Fig.9(f). Moreover, the q-SPICE and wideband q-SPICE approaches can suppress the clutters well, and generate a more sparse result.

For these experiments, the q-SPICE approach requires a computational time of about 16 seconds to form Fig.9(e). In contrast, using the wideband q-SPICE with $B = 32$ bands, and $Q = 8$ sampling points for each activated band, this reduces to 5 seconds to obtain Fig.9(f).

Furthermore, we measure the difference between the results of the q-SPICE and wideband q-SPICE approaches with the relative error defined as

$$e = \frac{\left\| \hat{S}_0 - \hat{S}_1 \right\|_2^2}{\left\| \hat{S}_0 \right\|_2^2} \tag{42}$$

where $\hat{S}_0$ and $\hat{S}_1$ are the results obtained by the q-SPICE and wideband q-SPICE methods, respectively. It is shown that the relative error between the results shown by Fig.9(e) and Fig.9(f) is -30.6 dB. This demonstrates that the wideband q-SPICE method does not suffer more than marginal performance degradation for the real data processing using a stationary platform.

TABLE II
AIRBORNE EXPERIMENTAL PARAMETERS

Parameters	Values
Scanning velocity	$72°/s$
PRF	200 Hz
Height	300 m
Depression angle	20°
Flight velocity	47 m/s

C. Airborne forward-looking imaging

Airborne forward-looking radar imaging has many potential applications, such as aircrafts landing, material airdrop, and terrain awareness and avoidance. Unfortunately, the principle of a classic monostatic synthetic aperture radar (SAR) or Doppler beam sharpening (DBS) prevents high-resolution imaging in forward-looking direction. With the advantage of flexible imaging configuration, scanning radar has been of considerable interest in the airborne forward-looking applications.

The platform motion will bring three coupling effects. The first one is the well-known range migration. For a moving platform, the instantaneous slant distance between the target and the platform is changing during the antenna scanning period. Therefore, the azimuth echo of the target will be spread into several range cells. This prevents further processing of the echoes in azimuth using reconstruction methods. The second effect is the additive Doppler shift caused by the platform motion [41]. The third effect is that the along-track velocity will affect the instant scanning speed [42]. This may result in nonuniform angular sampling in azimuth. Therefore, for a moving platform, the azimuth signal model may not be strictly consistent with that of a stationary platform. Fortunately, with range migration correction techniques, the range migration can be successfully eliminated [43], [44]. Moreover, in the case of forward-looking radar imaging, the latter two coupling effects are marginal and can be neglected [3], [42]. Therefore, with range migration correction, the forward-looking signal model for a moving platform can be well approximated by the convolution model, which is consistent with that of a stationary platform. This indicates that the reconstruction methods based on (1) can be used to reconstruct the ground truth for forward-looking radar imaging also on a moving platform.

To demonstrate the effectiveness of the proposed method for airborne platform, we conducted an airborne forward-looking experiment at Pucheng airport, Xi'an. The X-band FMCW radar was fixed on the bottom of a transport aircraft, as shown in Fig.10(a). The aircraft flew over the airport in a straight line, and the radar sweeped the forward-looking region to obtain the real beam image of the airport. To collect multiple groups of real data, the aircraft repeated the flight in a circular track. The imaging mode is illustrated in Fig.10(b), and the main experimental parameters are presented in Table II.

There are several typical targets in a airport, including four aircrafts, one vehicle, and one hangar, as shown by Fig.10(b) (ground view). Fig.11(a) presents the aerial view of the scenario. We note that there are no vehicles in Fig.11(a), as the photo is taken at different time. It is difficult to distinguish the targets from the real beam image because of the coarse azimuth resolution, as shown in Fig.11(b). Although the IAA and IAA-R can improve the azimuth resolution, the methods both suffer from high sidelobes, and background clutter that cannot be well suppressed, as shown in Fig.11(c) and Fig.11(d). In contrast, the q-SPICE and wideband q-SPICE approaches can provide more spare results, where the background clutter is better suppressed and the azimuth resolution is much higher, as shown in Fig.11(e) and Fig.11(f).

The q-SPICE method requires about 10 seconds to produce the result shown in Fig.11(e), whereas the wideband q-SPICE approach only require 4 seconds produce the result shown in Fig.11(f) for $B = 64$ bands, and $Q = 4$. The relative error of -36.5 dB between Fig.11(e) and Fig.11(f), computed using (42) indicates that the wideband q-SPICE method does not suffer noticeable performance degradation for the real data processing on the moving platform.

VI. CONCLUSION

This paper introduces a wideband q-SPICE method allowing for a computationally efficient estimation of sparse signals. Using integrated dictionaries, it is shown that the dimension of the parameter space can be reduced significantly. In the subsequent screening procedure, a smaller and zoomed dictionary with finer grid makes the wideband q-SPICE method perform more efficiently than the conventional q-SPICE method. This results in a reliable sparse signal reconstruction, at a much lower computational cost than earlier presented estimators.

REFERENCES

[1] J. Guan, J. Yang, Y. Huang, and W. Li, "Maximum a posteriori-based angular superresolution for scanning radar imaging," *IEEE Trans. Aerosp. Electron. Syst.*, vol. 50, no. 3, pp. 2389–2398, Jul. 2014.

[2] S. Uttam and N. A. Goodman, "Superresolution of coherent sources in real-beam data," *IEEE Trans. Aerosp. Electron. Syst.*, vol. 46, no. 3, pp. 1557–1566, Jul. 2010.

[3] L. Liu, X. Dong, J. Zhu, and D. Zhu, "An improved adaptive regularization method for forward looking azimuth super-resolution of a dual-frequency polarized scatterometer," *IEEE J. Sel. Top. Appl. Earth Obs. Remote Sens.*, vol. 9, no. 6, pp. 2145–2159, Jun. 2016.

[4] M. Migliaccio and A. Gambardella, "Microwave radiometer spatial resolution enhancement," *IEEE Trans. Geosci. Remote Sens.*, vol. 43, no. 5, pp. 1159–1169, May 2005.

[5] Y. Zhang, Y. Zhang, W. Li, Y. Huang, and J. Yang, "Super-resolution surface mapping for scanning radar: Inverse filtering based on the fast iterative adaptive approach," *IEEE Trans. Geosci. Remote Sens.*, vol. 56, no. 1, pp. 127–144, Jan. 2018.

[6] Y. Zhang, W. Li, Y. Zhang, Y. Huang, and J. Yang, "A fast iterative adaptive approach for scanning radar angular superresolution," *IEEE J. Sel. Topics Appl. Earth Observ. Remote Sens.*, vol. 8, no. 11, pp. 5336–5345, Nov. 2015.

[7] A. Gambardella and M. Migliaccio, "On the superresolution of microwave scanning radiometer measurements," *IEEE Geosci. Remote. S.*, vol. 5, no. 4, pp. 796–800, Oct. 2008.

[8] F. Lenti, F. Nunziata, M. Migliaccio, and G. Rodriguez, "Two-dimensional TSVD to enhance the spatial resolution of radiometer data," *IEEE Trans. Geosci. Remote Sens.*, vol. 52, no. 5, pp. 2450–2458, May 2014.

[9] D. Schiavulli, F. Nunziata, G. Pugliano, and M. Migliaccio, "Reconstruction of the normalized radar cross section field from GNSS-R delay-Doppler map," *IEEE J. Sel. Top. Appl. Earth Obs. Remote Sens.*, vol. 7, no. 5, pp. 1573–1583, May 2014.

[10] D. G. Long and D. L. Daum, "Spatial resolution enhancement of SSM/I data," *IEEE Trans. Geosci. Remote Sens.*, vol. 36, no. 2, pp. 407–417, Mar. 1998.

[11] D. G. Long, M. W. Spencer, and E. G. Njoku, "Spatial resolution and processing tradeoffs for HYDROS: application of reconstruction and resolution enhancement techniques," *IEEE Trans. Geosci. Remote Sens.*, vol. 43, no. 1, pp. 3–12, Jan. 2005.

(a) (b)

Fig. 10. Experiment taken on a moving platform. (a) Airborne platform. (b) Forward-looking imaging mode and optical scenario (ground view).

[12] F. Lenti, F. Nunziata, C. Estatico, and M. Migliaccio, "On the spatial resolution enhancement of microwave radiometer data in Banach spaces," *IEEE Trans. Geosci. Remote Sens.*, vol. 52, no. 3, pp. 1834–1842, Mar. 2014.

[13] F. Lenti, F. Nunziata, C. Estatico, and M. Migliaccio, "Spatial resolution enhancement of Earth observation products using an acceleration technique for iterative methods," *IEEE Geosci. Remote. S.*, vol. 12, no. 2, pp. 269–273, Feb. 2015.

[14] R. Sethmann, B. A. Burns, and G. C. Heygster, "Spatial resolution improvement of SSM/I data with image restoration techniques," *IEEE Trans. Geosci. Remote Sens.*, vol. 32, no. 6, pp. 1144–1151, Nov. 1994.

[15] M. Piles, A. Camps, M. Vall-llossera, and M. Talone, "Spatial-resolution enhancement of SMOS data: A deconvolution-based approach," *IEEE Trans. Geosci. Remote Sens.*, vol. 47, no. 7, pp. 2182–2192, Jul. 2009.

[16] H. Dropkin and C. Ly, "Superresolution for scanning antenna," in *Proc. 1997 IEEE Nat. Radar Conf.*, Syracuse, USA, May 1997, pp. 306–308.

[17] K. Tan, W. Li, Y. Huang, and J. Yang, "Dual-channel fast iterative shrinkage-thresholding regularization algorithm for scanning radar forward-looking imaging," *J. Appl. Remote Sens.*, vol. 11, no. 1, p. 015008, Jan. 2017.

[18] Y. Zhang, Y. Wang, W. Li, Y. Huang, and J. Yang, "Scanning radar angular superresolution with fast standard Capon beamformer," in *Proc. IEEE Int. Geosci. Remote Sens. Symp.*, Milan, Italy, Jul. 2015, pp. 3111–3114.

[19] T. Yardibi, J. Li, P. Stoica, M. Xue, and A. B. Baggeroer, "Source localization and sensing: A nonparametric iterative adaptive approach based on weighted least squares," *IEEE Trans. Aerosp. Electron. Syst.*, vol. 46, no. 1, pp. 425–443, Jan. 2010.

[20] W. Roberts, P. Stoica, J. Li, T. Yardibi, and F. A. Sadjadi, "Iterative adaptive approaches to MIMO radar imaging," *IEEE J. Sel. Top. Signal Process.*, vol. 4, no. 1, pp. 5–20, Feb. 2010.

[21] Y. Zhang, Y. Zhang, Y. Huang, W. Li, and J. Yang, "Angular superresolution for scanning radar with improved regularized iterative adaptive approach," *IEEE Geosci. Remote. S.*, vol. 13, no. 6, pp. 846–850, Jun. 2016.

[22] D. L. Donoho and M. Elad, "Optimally sparse representation in general (nonorthogonal) dictionaries via l_1 minimization," *Proc. Natl. Acad. Sci.*, vol. 100, no. 5, pp. 2197–2202, Mar. 2003.

[23] R. Tibshirani, "Regression shrinkage and selection via the LASSO: a retrospective," *J. R. Stats. Soc.: Ser. B (Stats. Method.)*, vol. 73, no. 3, pp. 273–282, Apr. 2011.

[24] I. F. Gorodnitsky and B. D. Rao, "Sparse signal reconstruction from limited data using FOCUSS: A re-weighted minimum norm algorithm," *IEEE Trans. Signal Process.*, vol. 45, no. 3, pp. 600–616, Mar. 1997.

[25] D. P. Wipf and B. D. Rao, "Sparse Bayesian learning for basis selection," *IEEE Trans. Signal Process.*, vol. 52, no. 8, pp. 2153–2164, Aug. 2004.

[26] X. Tan, W. Roberts, J. Li, and P. Stoica, "Sparse learning via iterative minimization with application to MIMO radar imaging," *IEEE Trans. Signal Process.*, vol. 59, no. 3, pp. 1088–1101, Mar. 2011.

[27] P. Stoica, P. Babu, and J. Li, "New method of sparse parameter estimation in separable models and its use for spectral analysis of irregularly sampled data," *IEEE Trans. Signal Process.*, vol. 59, no. 1, pp. 35–47, Jan. 2011.

[28] J. Swärd, S. I. Adalbjörnsson, and A. Jakobsson, "Generalized sparse covariance-based estimation," *Signal Process.*, vol. 143, pp. 311 – 319, Feb. 2018.

[29] Y. Zhang, Y. Zhang, Y. Huang, J. Yang, and A. Jakobsson, "Sparse source location for real aperture radar using generalized sparse covariance fitting," in *IEEE Radar Conf.*, Seattle, USA, Jun. 2017, pp. 1069–1074.

[30] M. Xue, L. Xu, and J. Li, "IAA spectral estimation: Fast implementation using the Gohberg-Semencul factorization," *IEEE Trans. Signal Process.*, vol. 59, no. 7, pp. 3251–3261, Jul. 2011.

[31] J. Karlsson, W. Rowe, L. Xu, G. O. Glentis, and J. Li, "Fast missing-data IAA with application to notched spectrum SAR," *IEEE Trans. Aerosp. Electron. Syst.*, vol. 50, no. 2, pp. 959–971, Apr. 2014.

[32] G. O. Glentis and A. Jakobsson, "Time-recursive IAA spectral estimation," *IEEE Signal. Proc. Let.*, vol. 18, no. 2, pp. 111–114, Feb. 2011.

[33] G. O. Glentis and A. Jakobsson, "Efficient implementation of iterative adaptive approach spectral estimation techniques," *IEEE Trans. Signal Process.*, vol. 59, no. 9, pp. 4154–4167, Sept. 2011.

[34] G. O. Glentis and A. Jakobsson, "Superfast approximative implementation of the IAA spectral estimate," *IEEE Trans. Signal Process.*, vol. 60, no. 1, pp. 472–478, Jan. 2012.

[35] A. Jakobsson, G. Glentis, and E. Gudmundson, "Computationally efficient time-recursive IAA-based blood velocity estimation," *IEEE Trans. Signal Process.*, vol. 60, no. 7, pp. 3853–3858, Jul. 2012.

[36] J. R. Jensen, G. O. Glentis, M. G. Christensen, A. Jakobsson, and S. H. Jensen, "Fast LCMV-based methods for fundamental frequency estimation," *IEEE Trans. Signal Process.*, vol. 61, no. 12, pp. 3159–3172, Jun. 2013.

[37] K. Angelopoulos, G.-O. Glentis, and A. Jakobsson, "Computationally efficient sparsity-inducing coherence spectrum estimation of complete

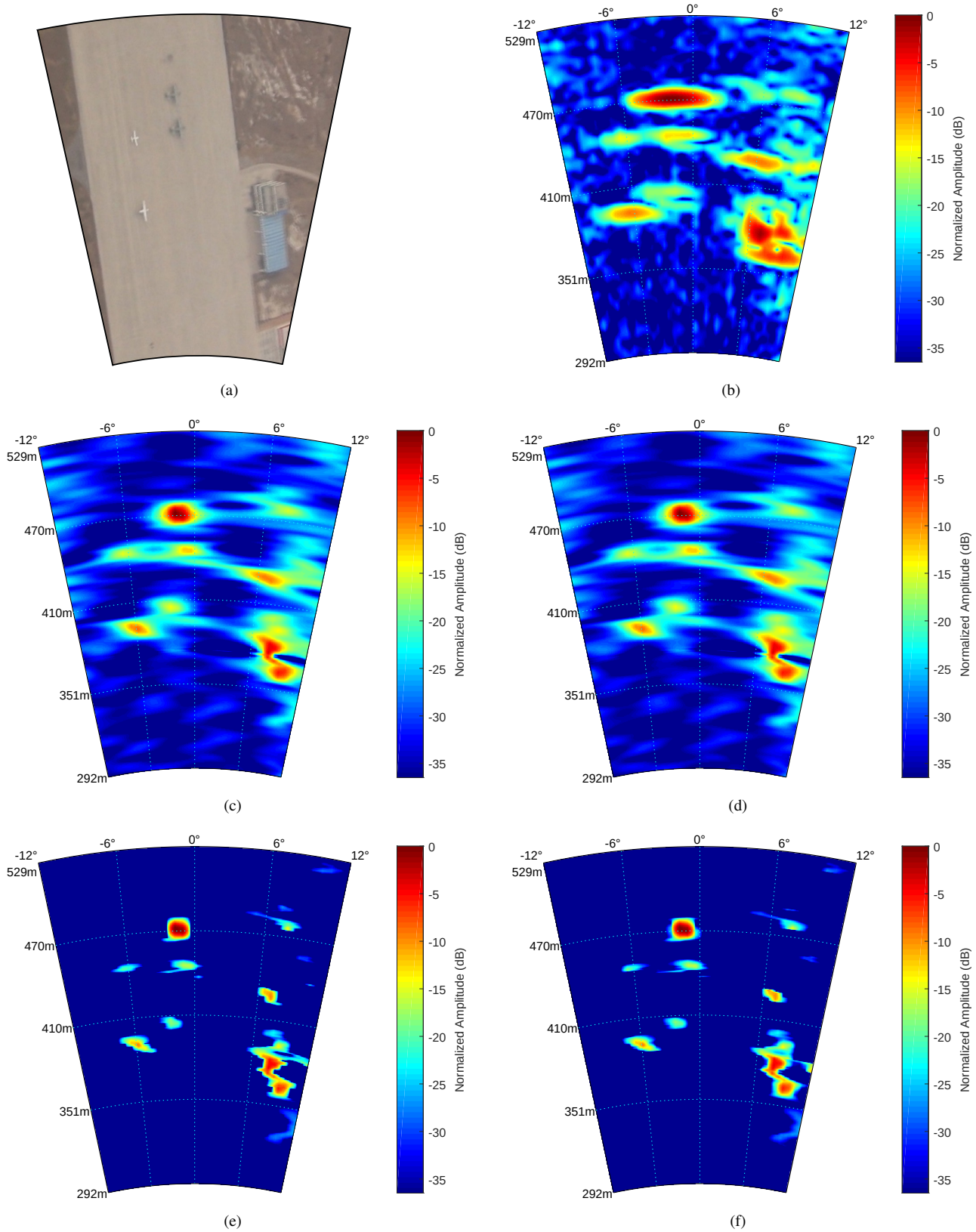

Fig. 11. Experiment taken on a moving platform. (a) Optical scenario taken from Google maps. (b) Real beam image after matched filtering in range. (c) Reconstruction result with the IAA. (d) Reconstruction result with the IAA-R. (e) Reconstruction result with the q-SPICE method ($q = 2$). (f) Reconstruction with the wideband q-SPICE method ($q = 2$).

and non-complete data sets," *Signal Process.*, vol. 93, no. 5, pp. 1221–1234, May 2013.

[38] M. Butsenko, J. Swärd, and A. Jakobsson, "Estimating sparse signals using integrated wideband dictionaries," to appear in *IEEE Trans. Signal Process.*.

[39] G. W. Stimson, *Introduction to Airborne Radar*, 2nd ed. Mendham, NJ: SciTech, 1998.

[40] P. Stoica, P. Babu, and J. Li, "SPICE: A sparse covariance-based estimation method for array processing," *IEEE Trans. Signal Process.*, vol. 59, no. 2, pp. 629–638, Feb. 2011.

[41] T. Long, Z. Lu, Z. Ding, and L. Liu, "A DBS Doppler centroid estimation algorithm based on entropy minimization," *IEEE Trans. Geosci. Remote Sens.*, vol. 49, no. 10, pp. 3703–3712, Oct. 2011.

[42] L. Chao, H. Yulin, and Y. Jianyu, "Establishment and analysis of accurate signal model for forward-looking imaging radar with motion platform," in *Proc. IET Int. Radar Conf.*, Xian, China, Apr. 2013, pp. 1–5.

[43] W. Li, J. Yang, and Y. Huang, "Keystone transform-based space-variant range migration correction for airborne forward-looking scanning radar," *Electron. Lett.*, vol. 48, no. 2, pp. 121–122, Jan. 2012.

[44] W. Li, J. Yang, Y. Huang, and J. Wu, "A geometry-based Doppler centroid estimator for bistatic forward-looking SAR," *IEEE Geosci. Remote. S.*, vol. 9, no. 3, pp. 388–392, May 2012.

Yongchao Zhang (S'15) received the B.S. degree in electronic information engineering from Hainan University, Haikou, China, in 2011. Currently, he is pursuing the Ph.D. degree at University of Electronic Science and Technology of China (UESTC), Chengdu, China. From 2016 to 2017, he was a visiting student at Lund University, Sweden.

His research interests include array signal processing and inverse problem in radar applications.

Andreas Jakobsson (S'95-M'00-SM'06) received his M.Sc. from Lund Institute of Technology and his Ph.D. in Signal Processing from Uppsala University in 1993 and 2000, respectively. Since, he has held positions with Global IP Sound AB, the Swedish Royal Institute of Technology, King's College London, and Karlstad University, as well as held an Honorary Research Fellowship at Cardiff University. He has been a visiting researcher at King's College London, Brigham Young University, Stanford University, Katholieke Universiteit Leuven, and University of California, San Diego, as well as acted as an expert for the IAEA. He is currently Professor and Head of Mathematical Statistics at Lund University, Sweden. He has published his research findings in about 200 refereed journal and conference papers, and has filed five patents. He has also authored a book on time series analysis (Studentlitteratur, 2013 and 2015), and co-authored (together with M. G. Christensen) a book on multi-pitch estimation (Morgan & Claypool, 2009). He is a member of The Royal Swedish Physiographic Society, a member of the EURASIP Special Area Team on Signal Processing for Multisensor Systems (2015-), and an Associate Editor for Elsevier Signal Processing. He has previously also been a member of the IEEE Sensor Array and Multichannel (SAM) Signal Processing Technical Committee (2008-2013), an Associate Editor for the IEEE Transactions on Signal Processing (2006-2010), the IEEE Signal Processing Letters (2007-2011), the Research Letters in Signal Processing (2007-2009), and the Journal of Electrical and Computer Engineering (2009-2014). His research interests include statistical and array signal processing, detection and estimation theory, and related application in remote sensing, telecommunication, and biomedicine.

Yin Zhang (S'13-M'17) received the B.S. and Ph.D. degrees in electronic information engineering from University of Electronic Science and Technology of China (UESTC), Chengdu, China, in 2008 and 2016, respectively. From 2015 to 2016, he was a visiting student at University of Delaware, USA. Currently, he is an associate research fellow with the School of Electronic Engineering, UESTC.

His research interests include radar imaging and signal processing in related radar applications.

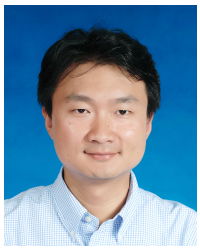

Yulin Huang (M'08) received the B.S. and Ph.D. degrees in electronic engineering from the University of Electronic Science and Technology of China (UESTC), Chengdu, China, in 2002, and 2008, respectively. From 2013 to 2014, he was a visiting researcher at University of Houston, USA. Since 2016, he has been a Professor with the School of Electronic Engineering, UESTC.

Dr. Huang has authored more than 80 journal and conference papers. He is also a member of the IEEE Aerospace and Electronic Systems Society. His research interests include synthetic aperture radar, target detection and recognition, artificial intelligence and machine Learning.

Jianyu Yang (M'91) received the B.S. degree from the National University of Defense Technology, Changsha, China, in 1984, and the M.S. and Ph.D. degrees from the University of Electronic Science and Technology of China (UESTC), Chengdu, in 1987 and 1991, respectively. In 2005, he visited Massachusetts Institute of Technology, USA. Since 1999, he has been a Professor with the School of Electronic Engineering, UESTC.

Dr. Yang has authored more than 120 journal and conference papers. He is a senior member of the Chinese Institute of Electronics. His research interests are mainly in synthetic aperture radar and statistical signal processing.